

Delayed polarization dynamics in Nd³⁺-doped yttrium-aluminum-garnet lasers

Guy Verschaffelt,* Guy Van der Sande, and Jan Danckaert

Department of Applied Physics and Photonics (IR-TONA), Vrije Universiteit Brussel, Pleinlaan 2, 1050 Brussels, Belgium

Bernard Ségard and Pierre Glorieux

Laboratoire de Physique des Lasers, Atomes et Molécules, Université des Sciences et Technologies de Lille, CNRS, UMR 8523, Villeneuve d'Ascq, F-59655 France

Thomas Erneux

Optique Nonlinéaire Théorique, Université Libre de Bruxelles, Campus Plaine, C.P. 231, 1050 Bruxelles, Belgium

(Received 7 December 2007; published 2 June 2008)

The response of a Nd³⁺-doped yttrium-aluminum-garnet laser is examined experimentally when the pump polarization direction is abruptly changed from one to the other stress-induced principal axis of the cavity. As a result, the laser output polarization changes direction but only after a significant delay. We numerically solve rate equations that describe the evolution of the two polarization fields coupled to the population inversion. The simulations indicate that the polarization switching (PS) delay depends on two successive processes that we analyze using multi-time-scale techniques. The analysis predicts two qualitatively different PS responses depending on how close the laser is from its threshold. Finally, we compare quantitatively the experimental and theoretical estimates of the PS delay.

DOI: [10.1103/PhysRevA.77.063801](https://doi.org/10.1103/PhysRevA.77.063801)

PACS number(s): 42.55.Rz, 42.60.Fc, 42.25.Ja

I. INTRODUCTION

Large polarization selectivity is desired in most lasers because inhibiting polarization dynamics improves the stability of the laser. The laser output can, e.g., be forced to be linearly polarized by introducing polarization selective elements (such as Brewster windows) inside the laser cavity. However, many lasers nowadays have a monolithic device structure and hence their cavity is quasi-isotropic. As a result, polarization selection is not easily achieved and the polarization state of the emitted light may change depending on externally imposed conditions (stress, magnetic field) or internally related parameters (pumping, hyperfine structure, local electric field). The question of the origin and of the dynamics of the laser polarization in quasi-isotropic structures has been investigated in different contexts. It started in the early days of the laser when it was observed that Earth's magnetic field could alter the polarization of light emitted by quasi-isotropic He-Ne lasers [1–3]. The question of which polarization is emitted by a laser was revived when doped fiber lasers were developed. These lasers use optical fibers that are isotropic except for stress induced (residual or introduced on purpose) birefringence [4–8]. Polarization selection was also an important issue in the development of vertical-cavity surface-emitting lasers (VCSELs). VCSELs often switch from one polarization state to the orthogonal one as their pump power is increased [9–14]. In all of these situations, the polarization dynamics strongly depends on the pumping mechanism, on the nature of the active medium, and on the design of the laser cavity. Electrical pumping as used in VCSELs, or in the discharge for a He-Ne laser, generates a population inversion that is evenly distributed

among spin sublevels. Optical pumping, as in fiber and in most solid state lasers, is usually achieved using polarized pump light. The polarized pump beam may introduce a preferred direction in the active medium. In atomic lasers (He-Ne, He-Xe), the nature of the atomic sublevels and their interaction with magnetic fields plays a key role in the selection of the polarization state of the laser output, leading to quite different behaviors, e.g., 3.39 μm and 0.6328 μm He-Ne laser transitions. In semiconductor lasers, the San Miguel–Feng–Moloney model shows that it is necessary to take into account the hyperfine level substructure in order to explain the laser's polarization [15], but many other effects (stress, temperature, etc.) also play a role [16]. The situation is by far more complicated in solid state lasers in which the active medium is made of doping ions inserted in amorphous (optical fiber) or crystalline (YAG, YVO₄, etc.) materials [6,17,18]. In such crystals, the site distribution of the active ions results in polarization-dependent absorption and emission mechanisms [5]. Polarization properties of Nd³⁺:YAG lasers have already been studied in the microchip and in the bulk configurations but they all concentrated on steady states. A yttrium-aluminum-garnet (YAG) laser's polarization depends on the pump beam's polarization and the stress-induced birefringence which determines the direction of the cavity polarization eigenmodes and their frequency difference [5,19,20]. By controlling the pump polarization and strength, the laser output can be linearly polarized or both polarization modes can be active simultaneously [21]. Also the possibility of a circularly polarized output beam has been studied [22].

In the present work, we investigate the polarization dynamics of a diode pumped Nd³⁺:YAG. More specifically, we study the dynamics induced by a sudden change of the polarization direction of a linearly polarized pump. Because Nd³⁺ ions are located in specific sites of the crystal, the absorption of linearly polarized light produces anisotropy in the

*guy.verschaffelt@vub.ac.be; <http://www.tona.vub.ac.be>

population inversion, i.e., it results in an inhomogeneous distribution of this population between the different Stark sublevels induced by the local electric field which is site dependent. Similarly, the population in the upper levels of the active medium is inhomogeneously distributed among the relevant hyperfine sublevels, leading to gain anisotropy. This gain medium anisotropy induced by linear pumping, together with the optical cavity anisotropy due to stress-induced birefringence may lead to complicated dynamics. In this paper we focus on a relatively simple case where the pump polarization initially coincides with one of the polarization eigenmodes of the optical cavity. The YAG laser is pumped slightly above threshold so that only one mode is active. We then monitor the laser's output as the pump polarization direction is suddenly rotated by 90° , providing a change in the gain anisotropy and inducing a transition to the orthogonal polarization state of the YAG laser. We show that the resulting polarization switching (PS) is considerably delayed with respect to the pump switching and exhibits relaxation oscillations (RO). Moreover, the switch-off of one linearly polarized mode and the switch-on of the other polarization mode may occur simultaneously or sequentially. Of particular physical interest is the multitime evolution of the PS transition that results from the interaction between the population inversion and the two polarization components of the YAG laser field. Modeling of such experimental results requires extended rate equations that account for the various sources of anisotropy. Several models were proposed to describe the steady states of quasi-isotropic Nd^{3+} :YAG lasers in the presence of absorption and gain anisotropy [5,7,8,20,23]. Here, an analytical theory of the observed dynamics is proposed on the basis of a multiscale analysis of the simplest of these models. We obtain quantitative agreement between the experimental observations and the predictions of this model.

This paper is organized as follows. In Sec. II, we introduce the experimental setup used to modulate the pump polarization and describe the PS phenomenon in a Nd^{3+} :YAG laser. We discuss the experimental results in terms of the pump power. Section III is devoted to the numerical simulations of the PS experiment using the four laser rate equations. We identify two qualitatively different PS transitions depending on how close the laser is from its threshold. We also investigate the important effect of the noise level on the PS delay. In Sec. IV, we analyze the PS transition as a delayed change of stability. We determine analytical expressions for the PS delay and compare it with the delay measured experimentally in Sec. V. Our main experimental and theoretical results are summarized and discussed in Sec. VI.

II. EXPERIMENTS

A. Polarization properties of a Nd^{3+} :YAG laser

The polarization properties of the radiation emitted by a Nd^{3+} :YAG laser with a quasi-isotropic cavity are best described using the polarization eigenmodes of the cavity. In the case of the laser used in our experiments, they are ruled by the stress-induced birefringence in the crystal. The two polarization eigenmodes are linearly polarized along orthogonal directions. Their associated frequencies are slightly

different due to the difference in the refractive indices along these two directions. In our experimental conditions this frequency difference is $\Delta\nu=5.52$ MHz.

The laser is pumped by a linearly polarized pump beam which is polarized at an angle ψ_p relative to one of the axes of the laser eigenmodes. The laser becomes active as the pump power P_{pump} exceeds a threshold P_{th} (≈ 92 mW in our experiments) that does not significantly depend on the pump polarization. The polarization state of the emitted field then depends on the value of ψ_p . In the following we concentrate on the cases where the pump polarization coincides with one of the laser eigenmodes' axes (i.e., $\psi_p=0^\circ$ or 90°). We observe the following sequence of phenomena as we progressively increase the pump power. At $P_{\text{pump}}=P_{\text{th}}$, laser emission starts in the linear polarization eigenmode parallel to the pump polarization. As the pump power exceeds a second threshold (at $P_{\text{pump}}\approx 185$ mW in our experiments), the second polarization eigenmode becomes active and the two polarization modes lase simultaneously with an optical frequency difference $\Delta\nu$ between the polarization modes. In our experiments, the pump power is always kept below the second threshold. The laser initially rests at a stable linearly polarized state when the pump polarization direction ψ_p is quickly switched from 0° to 90° . We monitor the total intensity and the laser emission in both polarization eigenmodes simultaneously.

B. Setup and device description

We use a Nd^{3+} :YAG laser emitting at 1064 nm in a single longitudinal and transverse mode. The active medium is a 5-mm-thick YAG crystal doped with Nd^{3+} ions. The laser cavity of length $L_{\text{opt}}\approx 30$ mm is bounded at one side by a dielectric mirror deposited on the YAG crystal and an external spherical mirror at the other side (with 80 mm radius of curvature). The mirror reflectivity is larger than 99% for the mirror deposited on the laser crystal and is 94% for the spherical coupling mirror. The laser is longitudinally pumped by a fiber coupled semiconductor laser operating at 808 nm. The pump light from the 100 μm core multimode fiber is first collimated and next sent through a polarizer, an electro-optic modulator (LINOS LM 0202), and a half-wave plate to obtain a linearly polarized pump beam of controlled polarization direction and intensity. This pump beam is focused inside the active crystal by a converging lens. The orientation of the half-wave plate is such that the pump azimuth coincides with one of the stress-induced birefringence axis of the active region. By changing the voltage across the electro-optic modulator, we can switch the direction of the pump polarization from 0° to 90° and vice versa. For that purpose, we apply a low-frequency (~ 0.5 kHz) square-wave modulation to the electro-optic modulator. We measured the time constant of the electro-optic modulator to be 3 μs , which is mainly determined by the high-power amplifier that we use to convert our low-level modulation signal into a suitable driving amplitude for the modulator. Throughout the rest of this paper, we denote by a (E_a) the polarization eigenmode (field) that is emitted for a voltage V_a of 0 V across the electro-optic modulator. The corresponding azimuth of the

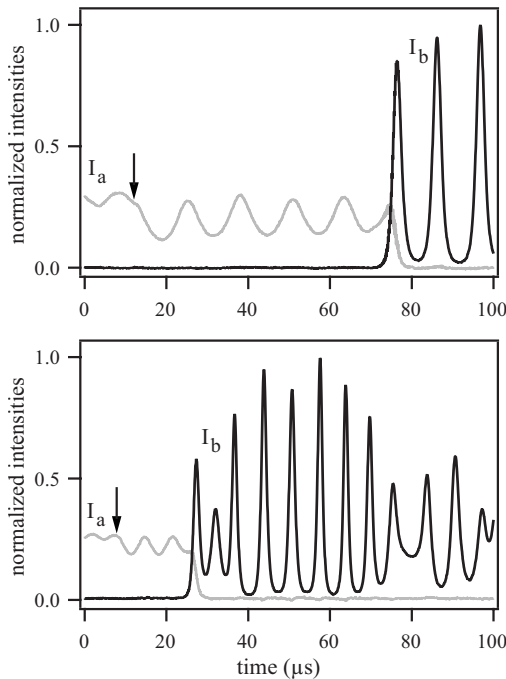


FIG. 1. Typical time trace of the intensity of E_a (gray) and E_b (black) at a pump strength $J=1.27$ (top) and $J=1.77$ (bottom). The pump azimuth ψ_p is changed from 0° to 90° at the time indicated by an arrow.

linearly polarized pump beam is taken to be $\psi_p=0^\circ$. Similarly, we denote by b (E_b) the polarization mode (field) that is emitted when the electro-optic modulator is biased at V_b such that it rotates the linearly polarized pump beam to $\psi_p=90^\circ$.

At the output side of the Nd³⁺:YAG laser, we use a series of beam splitters, half-wave plates, and polarizing beam splitters to measure the total and the polarization resolved intensity emitted by the Nd³⁺:YAG laser. These intensities are monitored using 150 MHz detectors (Thorlabs DET410), which are coupled either to a 10 kHz–3.5 GHz electrical spectrum analyzer to measure the RO frequency and the beat frequency between the polarization modes, or to a 500 MHz oscilloscope (Lecroy 334A) to record time traces.

C. Polarization switching experiments

We examine the response of the laser when the pump azimuth ψ_p is suddenly changed from 0° to 90° . In Fig. 1 (top) we plot the time trace of the polarization resolved intensity at a relative pump strength,

$$J \equiv \frac{P_{\text{pump}}}{P_{\text{th}}} = 1.27, \quad (1)$$

before and after the pump change. We note that the switching of the Nd³⁺:YAG laser's output polarization does not instantly follow the change in pump azimuth. Instead, the initially lasing mode E_a decreases sharply after changing the pump (see gray curve in Fig. 1). E_b only switches on after a delay of $\sim 61 \mu\text{s}$. We define the PS delay as the time lag between the change of the pump azimuth and the switch-on

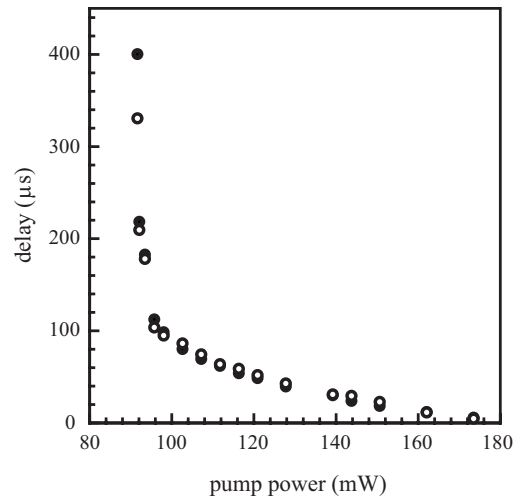


FIG. 2. PS delay when the pump azimuth is changed from 0° to 90° (dots) and when the pump azimuth is changed from 90° to 0° (open circles) as a function of the pump strength.

of E_b . During the interval between the initial change of the pump azimuth and the switch-on of E_b , the laser stays in the E_a mode but the average intensity drops by approximately 25%. This drop in average intensity is accompanied by ROs of the intensity of the E_a mode. After the PS delay, the E_a mode switches off rapidly (within a few μs) while the E_b mode switches on. For a time duration of 150–200 μs the switch-on of E_b shows large intensity ROs similar to what can be observed during a turn-on experiment.

To demonstrate the effect of the pump strength on the polarization switching, we show in Fig. 1 (bottom) the laser response for $J=1.77$. Again, the average intensity of the E_a mode drops when the pump azimuth is changed but the output polarization only follows the pump azimuth after a delay of 16.5 μs . This delay is much shorter than the one observed at $J=1.27$ indicating that the pump strength has a major effect on the PS delay. Note that the pump strength J always remains below the second threshold which occurs at $J \approx 2.0$.

The effect of the pump strength J on the switching delay is further investigated in Fig. 2. The delay decreases monotonically when increasing the pump strength and it diverges near the laser threshold. So far, we have only considered the change of the pump azimuth from 0° to 90° . The polarization behavior in the reverse switching scenario, i.e., when changing the pump azimuth from 90° to 0° , is completely similar. In that case, the average intensity of the E_b mode drops after the change in pump azimuth and this is accompanied by ROs in E_b . The E_a mode then turns on after a delay of several μs . In Fig. 2 we also plot the measured delay for this switching scenario. Again the measurements do not explore the vicinity of the second threshold.

In summary, we have found experimentally that our Nd³⁺:YAG laser immediately responds to a change in the pump polarization direction as the average intensity of the initial state changes. But the effective PS appears only after a considerable delay. This delay is independent of the direction in which we change the pump azimuth (i.e., from 0° to 90° or from 90° to 0°) but decreases if we increase the pump strength. In order to understand the basic physical mecha-

nisms responsible for this delayed transition, we shall investigate the laser rate equations in detail.

III. NUMERICAL SIMULATIONS

We have observed that the expected PS occurs after a delay. The main objective of this section is to obtain a numerical understanding of the PS phenomenon. For this purpose, we use a rate-equation model that has previously been successfully used to describe the steady-state properties of quasi-isotropic Nd³⁺:YAG laser [20,24]. We will show that this model can also reproduce our PS experiments.

A. Rate equations

The rate-equation model has been developed from earlier model equations [6–8] in order to describe the polarization of single longitudinal mode lasers pumped by a linearly polarized beam with a minimum set of equations. A more sophisticated model has been proposed in [23] but that model involves more equations and is not suited for the analytical treatment presented in Sec. IV. As the pump polarization is either 0° or 90°, the equations by Bouwmans *et al.* [20,24] simplify as

$$\frac{dE_a}{dt} = [N_0(1 + \beta_L) + N_c(1 - \beta_L) - 1]E_a + \delta, \quad (2)$$

$$\frac{dE_b}{dt} = [N_0(1 + \beta_L) - N_c(1 - \beta_L) - 1]E_b + \delta, \quad (3)$$

$$\frac{dN_0}{dt} = \gamma \left[A_0 - N_0 \left(1 + \frac{1 + \beta_L}{2} (E_a^2 + E_b^2) \right) - N_c \frac{1 - \beta_L}{2} (E_a^2 - E_b^2) \right], \quad (4)$$

$$\frac{dN_c}{dt} = \gamma \left[A_c - N_0 \frac{1 - \beta_L}{4} (E_a^2 - E_b^2) - N_c \left(1 + \frac{1 + \beta_L}{2} (E_a^2 + E_b^2) \right) \right]. \quad (5)$$

In these equations, E_a and E_b are the amplitudes of the electric field along the cavity polarization eigenmodes, N_0 and N_c are the first two Fourier components which take into account the dependence of the population inversion on the azimuth (N_0 is the continuous component). Time t is measured in units of κ^{-1} where κ is the field decay rate in the laser cavity. $\gamma \equiv \gamma_{||} / \kappa$ is defined as the ratio of the population and cavity decay rates. The Fourier components of the pumping rate are given by

$$A_0 = A(1 + \beta_p) \quad \text{and} \quad A_c = \frac{A}{2}(1 - \beta_p)\cos(2\psi_p), \quad (6)$$

where ψ_p is the angle between the directions of the pump polarization and the E_a polarization mode. A is the normalized pump strength. The parameters β_p and β_L were previously introduced in [5,8,17] and account for the anisotropy

of the pump absorption and the gain, respectively. Both result from the mechanisms that generate pump-induced anisotropy as explained in the introduction. The value of these parameters is between 0 (maximum anisotropy) and 1 (no anisotropy). Because E_a and E_b may approach exponentially small values [$\exp(-1/\gamma)$], a small constant term (δ) is added to the right-hand sides of Eqs. (2) and (3). This term minimally describes the effect of noise which is important in our experiments. It corresponds to spontaneous emission which is significant for our laser, but also to diverse perturbations, in particular those introduced by the mechanical alignment accuracy in the pump azimuth switching device. A value of $\delta = 10^{-5}$ best fits our PS experiments but the effect of decreasing δ will be analyzed in detail in Sec. III C.

Before we analyze the PS phenomenon, it is worthwhile to emphasize some particular features of these rate equations. From (2) and (3), we note that the growth rates of E_a and E_b differ by the sign of the coefficient multiplying N_c . This means that the growth rates of E_a and E_b are different and a change of stability of the $E_a \neq 0$ steady state resulting from changing ψ_p does not necessarily imply the growth of E_b from zero. If $\beta_L = 1$, there is no gain difference between the cavity polarization eigenmodes. In that case both modes would be active above lasing threshold and the total intensity of the emitted field would be randomly distributed among them for all values of the pump strength and azimuth. Such a situation has not been observed in our devices. Furthermore, we note that if $\beta_p = 1$, $A_c = 0$ from (6), and the PS experiment is no longer possible since ψ_p no longer appears in Eq. (5). Small anisotropies are thus essential for the success of a PS transition.

The steady-state solutions have been determined in [20,24] and we summarize the main results. Equations (2)–(5) admit three nonzero steady-state solutions, namely (i) the E_a single-mode solution, (ii) the E_b single-mode solution, and (iii) the E_a and E_b mixed-mode solution. The first (second) single-mode steady state is stable if the pump azimuth ψ_p is equal to 0° (equal to 90°) and if A is larger than A_1 defined by

$$A_1 \equiv \frac{2}{3 + \beta_L + \beta_p + 3\beta_L\beta_p}. \quad (7)$$

The third mixed-mode steady state where both E_a and E_b are lasing is stable if A is larger than A_2 defined by

$$A_2 \equiv \frac{(-1 + \beta_L)}{2(1 + \beta_L)(\beta_L - \beta_p)}. \quad (8)$$

For A_2 to be positive, it is required that $0 \leq \beta_L < \beta_p \leq 1$. In this paper, we consider the range $A_1 < A < A_2$ and concentrate on the PS transition between the E_a and E_b states as ψ_p is quickly changed from 0° to 90°. Finally, we need to specify how A is related to the experimental pump strength P and pump threshold P_{th} . This relation is given by

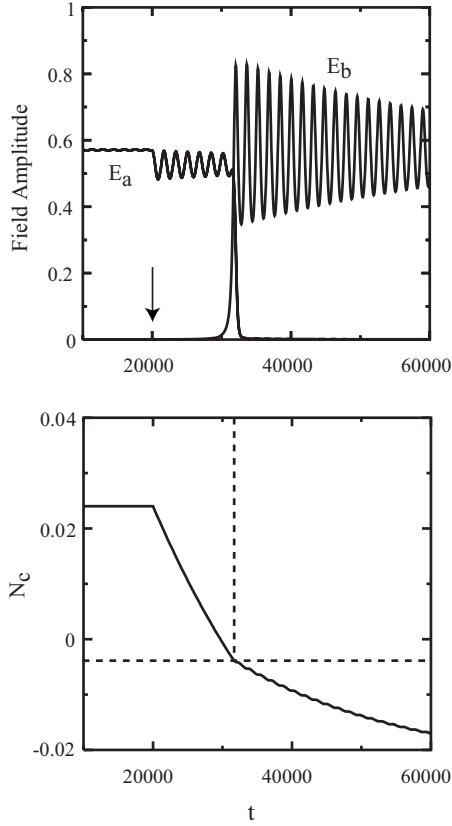


FIG. 3. Simulated evolution of the two polarization fields E_a and E_b (top) and population N_c (bottom). The values of the fixed parameters are $\beta_L=0.59$, $\beta_P=0.77$, $\gamma=3 \times 10^{-5}$, and $J=1.27$. The laser is initially at its stable single polarization state $E_a \approx 0.57$ and $E_b=0$. The arrow indicates the time at which ψ_P is instantaneously changed from 0° to 90° . The expected PS transition appears after a delay $\Delta t \approx 11\,500$. Note the change of slope of N_c at the PS transition. It occurs at a slightly negative value of N_c . If δ progressively increases from zero, this value of N_c approaches zero.

$$A = \frac{P}{P_{\text{th}}} A_1 = J A_1, \quad (9)$$

where J represents the relative pump strength ($J=J_1=1$ corresponds to the laser threshold $A=A_1$ and $J=J_2$ corresponds to the second threshold $A=A_2$).

B. Laser parameters

From the values of the mirror reflectivity and the optical length of the cavity, we estimate the field decay rate as $\kappa = 1.55 \times 10^8 \text{ s}^{-1}$. The population decay rate γ_{\parallel} is determined from measuring the relaxation oscillation frequency f of the total intensity for different values of the pump. Since $f^2 \approx \kappa \gamma_{\parallel} (P - P_{\text{th}})$, the slope of the best linear fit of the experimental data yields $\kappa \gamma_{\parallel} = 7.2 \times 10^{11} \text{ s}^{-2}$. Using then the calculated value of κ , we obtain $\gamma_{\parallel} = 4.65 \times 10^3 \text{ s}^{-1}$. This value corresponds to an excited-state lifetime of $215 \text{ }\mu\text{s}$ which is very close to the standard values ($230\text{--}250 \text{ }\mu\text{s}$) documented in the literature for similar crystals [25,26]. Knowing κ and γ_{\parallel} , we note that the ratio $\gamma = \gamma_{\parallel} / \kappa = 3.0 \times 10^{-5}$ is small, which

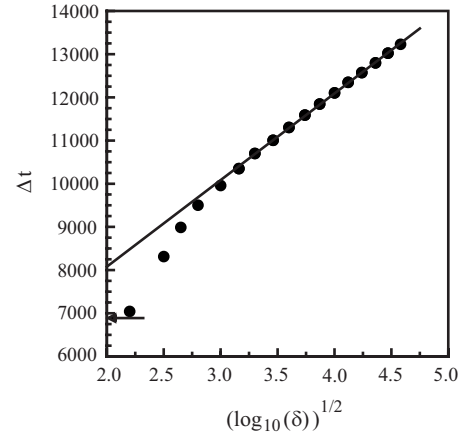


FIG. 4. Delay as a function of δ . The delay Δt is a linear function of $\sqrt{-\log_{10}(\delta)}$ provided δ is sufficiently small. The arrow indicates the critical value of δ for which $N_c=0$.

means that N_0 and N_c decay on a much slower rate than the fields in the cavity. In Sec. IV, we shall take advantage of this small value of γ and propose a multiple-time-scale analysis of Eqs. (2)–(5).

The anisotropy parameters β_L and β_P can be deduced from the steady-state properties of the laser emission. See [20,24] for details. Under our experimental conditions, we determine $\beta_L=0.59$ and $\beta_P=0.77$.

C. Numerical simulations

In order to understand what are the physical mechanisms responsible for the delayed PS, we have integrated Eqs. (2)–(5) numerically with the values of the parameters documented in the preceding section. We fixed δ to the value $\delta = 10^{-5}$ for which computed and experimental delays are in good quantitative agreement. The evolution of the two polarization fields and the population N_c is shown in Fig. 3. N_0 remains almost constant during the PS transition and is not shown.

After the instantaneous change of the pump azimuth ψ_P from 0° to 90° (arrow in Fig. 3 top), E_a exhibits ROs while E_b remains close to zero until it jumps to large amplitude ROs. We note from Fig. 3 bottom that N_c monotonically decays to its new state but exhibits almost no oscillations. The behavior shown in Fig. 3 suggests that the PS transition depends on two distinct time scales, namely $t_1 = \sqrt{\gamma} t$, the time scale of the ROs and $t_2 = \gamma t$, the decay rate of N_c . Recall that time t is dimensionless ($t \equiv \kappa t'$ where $\kappa = 1.55 \times 10^8 \text{ s}^{-1}$ and t' is the original time). We determine Δt as the time interval between the sudden change of the pump azimuth and the time at which $E_b > 10^{-2}$. The PS shown in Fig. 3 occurs with a delay $\Delta t \approx 11\,500$ implying $\Delta t' = 74 \text{ }\mu\text{s}$ (experimentally $\Delta t' = 61 \text{ }\mu\text{s}$).

The delay Δt of the PS transition strongly depends on the value of δ . In Fig. 4, we determine Δt as a function of δ and verify that Δt increases like $\sqrt{-\log_{10}(\delta)}$ as $\delta \rightarrow 0$. This effect is typical to slow passage problems through a bifurcation point and is explained in Sec. IV.

The time evolution of the simulated signals may be interpreted in terms of the quasisteady state that rules the dynam-

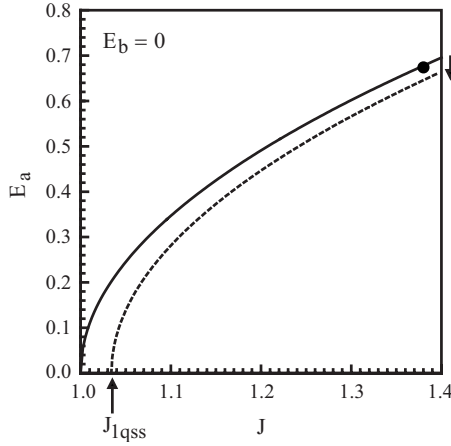


FIG. 5. Quasisteady state for E_a . As soon as the pump azimuth is changed, the stable steady state $E_a \neq 0$, $E_b = 0$ (full line) becomes unstable. But since E_b remains close to zero during a time interval Δt , E_a approaches a stable quasisteady state (broken line) provided $J > J_{1qss}$. If $J < J_{1qss}$, E_a jumps to zero.

ics of the delay (see Fig. 5). The steady-state solution for the single polarization state $E_a \neq 0$ and $E_b = 0$ admits a bifurcation point that satisfies the following equation:

$$A_c(1 - \beta_L) + (1 + \beta_L)A_0 - 1 = 0. \quad (10)$$

Using (6) with $\psi_p = 0$, we obtain $A = A_1$ previously defined by (7), or equivalently, using (9), $J = J_1 = 1$. As the pump azimuth changes ($\psi_p = 90^\circ$), A_c changes sign and E_a approaches a quasisteady state during the time interval where E_b still remains close to zero. See Fig. 5. This quasisteady state admits a new bifurcation point located at $A = A_{1qss}$ satisfying Eq. (10) now with $A_c < 0$. It is given by

$$A_{1qss} = \frac{2}{1 + 3\beta_L + 3\beta_P + \beta_L\beta_P} \quad (11)$$

or equivalently, using (9), $J = J_{1qss}$ where

$$J_{1qss} = \frac{3 + \beta_L + \beta_P + 3\beta_L\beta_P}{1 + 3\beta_L + 3\beta_P + \beta_L\beta_P}. \quad (12)$$

Note that the branch of quasisteady state for E_a after the change of the pump azimuth has a lower amplitude than the original branch. This explains why the E_a relaxation oscillations observed experimentally and numerically exhibit a lower average value compared to the initial state. For the same values of the fixed parameters used in Fig. 3, we find $A_1 \approx 0.35$, $A_{1qss} \approx 0.36$, and $A_2 \approx 0.72$ implying $J_1 = 1$, $J_{1qss} \approx 1.034$, and $J_2 \approx 2.05$.

Figure 6 illustrates the case $J_1 < J < J_{1qss}$ where E_a exhibits its PS transition before E_b and without ROs. The same values of the parameters as in Fig. 3 are used, except that $A = 0.36$ instead of $A = 0.44$. This regime has been observed experimentally close to the laser threshold and its evolution as we increase J will be described elsewhere.

In summary, our simulations of the laser rate equations reveal two qualitatively different PS transitions depending on how close we are from the laser threshold. The possible regimes are separated by a new steady-state bifurcation point

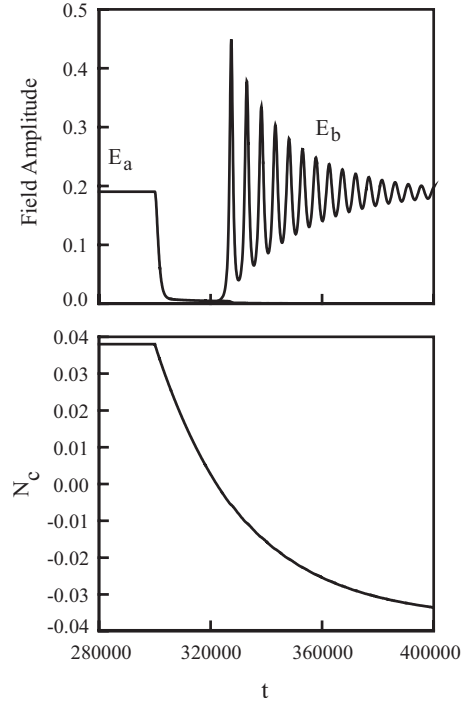


FIG. 6. The PS transition for $J_1 < J < J_{1qss}$. The exponential increase of E_b appears with a delay after E_a has jumped to zero.

(namely, $J = J_{1qss} > J_1 = 1$) that emerges as we change the pump azimuth.

IV. ANALYSIS

In this section, we analyze the solution of the laser equations before the PS appears. We need to consider the cases $J > J_{1qss}$ and $J \leq J_{1qss}$ separately because the stability conditions are different.

A. $J > J_{1qss}$

The numerical simulation shown in Fig. 3 indicates that $E_b(t)$ remains close to zero before it jumps while $E_a(t)$ exhibits ROs with a period proportional to $\gamma^{-1/2}$ and N_c slowly decreases on a γ^{-1} time scale. Furthermore, we note that the magnitude of N_c remains relatively small compared to E_a ($|N_c| \sim 10^{-2}$) which we attribute to the moderate value of $1 - \beta_L = 0.41$ and $1 - \beta_P = 0.23$. This is confirmed by the analytical expressions of the single polarization steady states indicating that N_c is proportional to $1 - \beta_L$ (assuming $1 - \beta_P$ and $1 - \beta_L$ on the same scale). A multiple-time-scale perturbation analysis that takes into account the small values of $1 - \beta_L$ and $1 - \beta_P$ is detailed in the Appendix so that we only summarize the main results.

After averaging the solution on the fast time scale $s \equiv \sqrt{2}\gamma t$, we find that $N_c = N_c(\sigma)$ is a slowly varying function of $\sigma \equiv \sqrt{\frac{2}{\gamma}}s$, in the first approximation, and that the leading approximations for the averages $\langle N_0 \rangle$ and $\langle E_a^2 \rangle$ are given by

$$\langle N_0 \rangle \approx \frac{1}{1 + \beta_L} \quad \text{and} \quad \langle E_a^2 \rangle \approx 2 \frac{A_0(1 + \beta_L) - 1}{1 + \beta_L}. \quad (13)$$

Substituting these expressions into the right-hand side of Eq. (5), we obtain

$$\frac{dN_c}{dt} \approx -\gamma A_0(1 + \beta_L)(N_c - N_{c+}), \quad (14)$$

where

$$N_{c+} = \frac{1}{A_0(1 + \beta_L)} \left(-|A_c| - \frac{(1 - \beta_L)}{2(1 + \beta_L)^2} [A_0(1 + \beta_L) - 1] \right) \quad (15)$$

is the approximation of the steady-state value of N_c after the switch. Equation (14) must be solved using the initial condition $N_c(0) = N_{c-}$, where

$$N_{c-} = \frac{1}{A_0(1 + \beta_L)} \left(|A_c| - \frac{(1 - \beta_L)}{2(1 + \beta_L)^2} [A_0(1 + \beta_L) - 1] \right) \quad (16)$$

is the approximation of the steady-state value of N_c before the switch. The solution of Eq. (14) is exponential and is given by

$$N_c = (N_{c-} - N_{c+}) \exp[-\gamma A_0(1 + \beta_L)t] + N_{c+}. \quad (17)$$

In order to determine when the PS transition appears, we examine Eq. (3) for E_b . If $\delta=0$, the change of stability of $E_b=0$ appears after a delay Δt defined as the root of

$$\int_0^{\Delta t} N_c(t) dt = 0. \quad (18)$$

On the other hand, if $\delta \gg \exp(-\gamma^{-1})$, the PS transition appears when

$$N_c(\Delta t) \approx 0. \quad (19)$$

Using (17), we obtain from the condition (19) the following expression for the PS delay:

$$\Delta t = -\frac{1}{\gamma A_0(1 + \beta_L)} \ln \left(\frac{-N_{c+}}{N_{c-} - N_{c+}} \right). \quad (20)$$

The critical time Δt determined from the integral condition (18) is marked by the vertical dashed line in Fig. 7. It compares well with the exponential increase of E_b obtained numerically from Eqs. (2)–(5) with $\delta=10^{-20}$ (point where N_c vs t changes slope). As δ is increased up to 10^{-5} , the actual increase of E_b occurs sooner and comes closer to the time where $N_c=0$ given by (20). This effect is typical to slow passage problems through bifurcation points [27]. Here the bifurcation point corresponds to a change of stability of $E_b=0$ assuming N_c as the bifurcation parameter. The bifurcation point occurs at $N_c=0$. The increase of the delay as $\delta \rightarrow 0$ is proportional to $\sqrt{-\log_{10}(\delta)}$ as verified in Fig. 4. The analytical prediction (20) is compared with the numerical and experimental estimates of the delay Δt in Sec. V.

B. $J \leq J_{1qss}$

The analysis leading to the expression (20) is only valid for $J > J_{1qss}$ implying $E_a^2 > 0$. If $J_1 \leq J_{1qss}$, $E_a=0$, and we need to take into account that both E_a and E_b are zero during the silent phase prior to the jump of E_b . The exact solution of

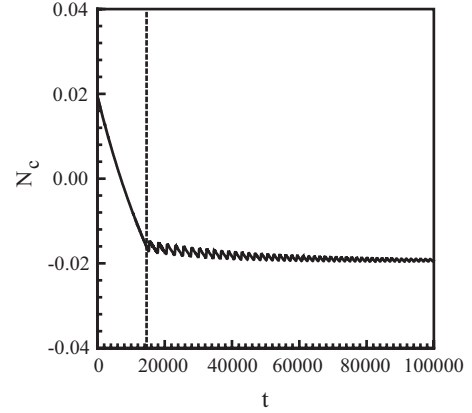


FIG. 7. The dashed line marks the critical time above which I_b increases exponentially. It is defined as the nonzero root of the integral condition. The actual numerical jump corresponds to the change of slope of N_c . A very small value of $\delta=10^{-20}$ was used in the numerical simulations. If δ is progressively increased from 10^{-20} to 10^{-5} , the jump occurs sooner and approaches the time when $N_c=0$.

Eqs. (4) and (5) with $\delta=0$ and $E_a^2=E_b^2=0$ are

$$N_0 = (N_{0-} - A_0) \exp(-\gamma t) + A_0, \quad (21)$$

$$N_c = (N_{c-} + |A_c|) \exp(-\gamma t) - |A_c|, \quad (22)$$

where N_{0-} and N_{c-} denote the steady-state values of N_0 and N_c before the switch. From Eq. (3), the change of stability of $E_b=0$ (with $\delta \neq 0$ sufficiently large) is

$$N_0(1 + \beta_L) - N_c(1 - \beta_L) - 1 = 0. \quad (23)$$

We substitute (21) and (22) into Eq. (23) and note that the expression $A_0(1 + \beta_L) + |A_c|(1 - \beta_L) - 1$ simplifies as

$$A_0(1 + \beta_L) + |A_c|(1 - \beta_L) - 1 = \frac{A}{A_1} - 1. \quad (24)$$

We analyze the condition (23) in the limit $A - A_1 \rightarrow 0$. We note that $N_{0-} - A_0$ is $O(A - A_1)$ small and that $N_{c-} + |A_c| \rightarrow 2|A_c| = A_1(1 - \beta_P)$. In the limit $A - A_1$ small, (23) simplifies as

$$-A_1(1 - \beta_P)(1 - \beta_L) \exp(-\gamma t) + \left(\frac{A}{A_1} - 1 \right) \approx 0 \quad (25)$$

and leads to the delay

$$\Delta t = -\frac{1}{\gamma} \ln \left(\frac{(A/A_1 - 1)}{A_1(1 - \beta_L)(1 - \beta_P)} \right) \quad (26)$$

which is proportional to $|\ln(A - A_1)|$.

V. QUANTITATIVE COMPARISONS

In Fig. 8, we compare the analytical approximations (20) and (26) with the experimental data. Best quantitative agreement is obtained by slightly changing the values of the parameters $(\gamma, \beta_P, \beta_L)$ from $(3 \times 10^{-5}, 0.77, 0.59)$ to $(3.3 \times 10^{-5}, 0.75, 0.62)$. We note the sudden increase of Δt as J is

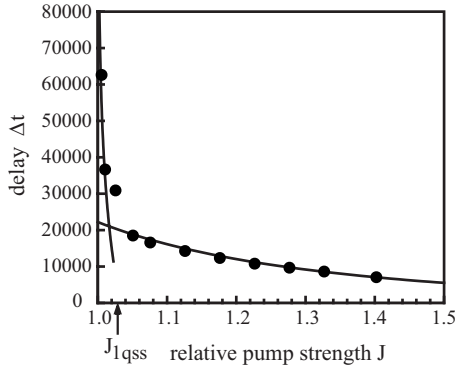


FIG. 8. Comparison between experimental (dots) and analytical (lines) delays. The values of the parameters are $\kappa=1.55 \times 10^8 \text{ s}^{-1}$, $\gamma=3.3 \times 10^{-5}$, $\beta_L=0.62$, and $\beta_P=0.75$.

decreased and passes J_{1qss} . To further investigate the transition between the far- and close-to-threshold regimes, we compare in Fig. 9 the analytical approximations (20) and (26) with the numerically computed delays using the original laser equations (2)–(5). We clearly note that the transition near $J=J_{1qss}$ is not discontinuous but is smooth. However, a detailed description of the transition layer near $J=J_{1qss}$ is beyond the scope of this paper. Finally, the good correspondence close to the second threshold (not shown) between the analytical delay (that does not take the proximity to the second threshold into account) and the simulations of the full model (which do contain any possible effects of the second threshold) shows that the proximity to the second threshold does not play a role in the polarization switching delay.

In summary, an asymptotic analysis of the rate equations based on the natural values of the laser parameters led to analytical expressions of the delay as a function of the pump strength J . In the first case ($J > J_{1qss}$), the delay depends on the relative change of the population inversion. It is equivalent to the expression of the turn-on time in single-mode gain switching experiments. In the second case ($J_1 < J < J_{1qss}$), the delay approaches infinity as we approach the laser threshold $J=J_1=1$. The analytical expressions compare quantitatively to the experimental and numerical observations.

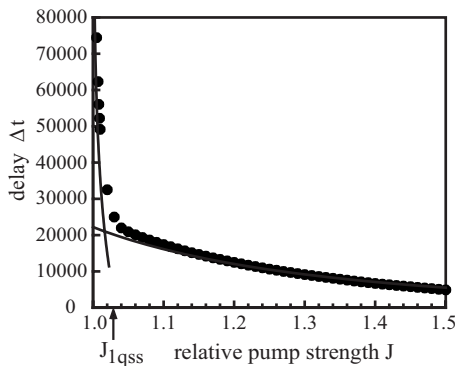


FIG. 9. Comparison between numerically computed (dots) and analytical (line) delays. The values of the parameters are $\kappa=1.55 \times 10^8 \text{ s}^{-1}$, $\gamma=3.3 \times 10^{-5}$, $\beta_L=0.62$, and $\beta_P=0.75$.

VI. CONCLUSIONS

We have studied both experimentally and analytically the polarization dynamics of a $\text{Nd}^{3+}:\text{YAG}$ laser emitting in a single longitudinal and transverse mode. The laser is pumped with a linearly polarized beam and the polarization angle is modulated using an electro-optic modulator. When we suddenly change the polarization angle of the pump beam by 90° , while keeping the pump amplitude constant, we observe that a new polarization mode appears after a delay of several tens of μs . After PS, the initial polarization intensity goes to zero while large amplitude relaxation oscillations of the orthogonal polarization intensity appear. Numerical simulations of rate equations reveal that the delay is the result of the slow recovery of the population inversion and that it depends on the noise level always present in experiments. An asymptotic analysis of the rate equations then emphasizes the effects of the anisotropies and the power strength.

Both the numerical and analytical studies reveal that there exist two qualitatively different PS experiments. The first and most general case is characterized by decaying ROs for both the initial and final states. It occurs for sufficiently large power strength and is studied in detail in this paper. The second case occurs near the laser threshold and is characterized by decaying ROs for only the final state. The detailed comparison between numerical and analytical approximations then suggests a transition layer regime where a smooth change of the two described PS behaviors is possible. This transition layer regime needs a new analysis of the laser rate equations and will be described elsewhere.

ACKNOWLEDGMENTS

This work was supported by the Belgian Science Policy Office through the Interuniversity Attraction Pole program. J.D., G.VdS., and G.V. acknowledge the FWO (Fund for Scientific Research–Flanders) for support. T.E. acknowledges the support of the Fonds National de la Recherche Scientifique. Also support from and discussions within the framework of the European COST action 288 is acknowledged.

APPENDIX: DELAYED PS

The purpose of this appendix is to show that (I_a, N_0) exhibits relaxation oscillations while N_c is slowly varying and determines the critical point where $I_b=0$ changes stability. For the algebraic clarity, we shall take advantage of the small values of $1-\beta_P$ and $1-\beta_L$.

1. Slow evolution of N_c

The laser rate Eqs. (2)–(5) with $E_b=0$ and $\psi_P=90^\circ$ describe the laser output after the pump switch. They are given by

$$\frac{dE_a}{dt} = [N_0(1 + \beta_L) + N_c(1 - \beta_L) - 1]E_a, \quad (\text{A1})$$

$$\frac{dN_0}{dt} = \gamma \left[A_0 - N_0 \left(1 + \frac{1 + \beta_L}{2} E_a^2 \right) - N_c \frac{(1 - \beta_L)}{2} E_a^2 \right], \quad (\text{A2})$$

$$\frac{dN_c}{dt} = \gamma \left[-\frac{A}{2} (1 - \beta_P) - N_0 \frac{(1 - \beta_L)}{4} E_a^2 - N_c \left(1 + \frac{1 + \beta_L}{2} E_a^2 \right) \right]. \quad (\text{A3})$$

We consider the time scale of the relaxation oscillations as our basic time scale and introduce

$$s = \sqrt{2\gamma}t \quad (\text{A4})$$

into the rate equations (A1)–(A3). Comparing left- and right-hand sides of Eq. (A1) then requires that N_0 deviates from its steady state by a quantity $\sqrt{\gamma}$. Therefore, we introduce the deviation n_0 defined by

$$N_0 = \frac{1}{1 + \beta_L} \left(1 + \sqrt{\frac{\gamma}{2}} n_0 \right). \quad (\text{A5})$$

The factor 2 in both (A4) and (A5) has been introduced for the mathematical clarity of the final equations. Note that $1 - \beta_L$ and $1 - \beta_P$ with $\beta_L = 0.59$ and $\beta_P = 0.77$ are relatively small and are of the same order of magnitude. Equation (A3) then suggests to rescale N_c as

$$N_c = (1 - \beta_L) n_c. \quad (\text{A6})$$

After inserting (A4)–(A6) into Eqs. (A1)–(A3), we obtain the following three equations for the intensity $I_a = E_a^2$, and the populations n_0 and n_c :

$$\frac{dI_a}{ds} = \left(n_0 + \sqrt{\frac{2}{\gamma}} (1 - \beta_L)^2 n_c \right) I_a, \quad (\text{A7})$$

$$\begin{aligned} \frac{dn_0}{ds} = & A_0(1 + \beta_L) - \left(1 + \frac{1 + \beta_L}{2} I_a \right) - \sqrt{\frac{\gamma}{2}} n_0 \left(1 + \frac{1 + \beta_L}{2} I_a \right) \\ & - n_c \frac{(1 - \beta_L)^2 (1 + \beta_L)}{2} I_a, \end{aligned} \quad (\text{A8})$$

$$\begin{aligned} \frac{dn_c}{ds} = & \sqrt{\gamma} \left[-\frac{A}{2} \frac{1 - \beta_P}{1 - \beta_L} - \frac{1}{1 + \beta_L} \frac{1}{4} \left(1 + \sqrt{\frac{\gamma}{2}} n_0 \right) I_a \right. \\ & \left. - n_c \left(1 + \frac{1 + \beta_L}{2} I_a \right) \right]. \end{aligned} \quad (\text{A9})$$

Equations (A7)–(A9) are equivalent to the original Eqs. (A1)–(A3). But, by introducing (A4) and (A5), we have removed the small parameter γ multiplying the right-hand side of Eq. (A2). The resulting Eqs. (A7) and (A8) for I_a and n_0 exhibit the laser relaxation oscillations as we shall now demonstrate. Before we do this, we take advantage of the small values of $1 - \beta_L$ and $1 - \beta_P$ by assuming

$$\beta_L = 1 + \gamma^{1/4} b_L \quad \text{and} \quad \beta_P = 1 + \gamma^{1/4} b_P. \quad (\text{A10})$$

The $\gamma^{1/4}$ power is motivated by the fact that we wish the second term on the right-hand side of Eq. (A7) to be $O(1)$. With the values of the parameters $\gamma = 3 \times 10^{-5}$, $\beta_L = 0.59$, and

$\beta_P = 0.77$, we determine $b_L \approx -5.5$ and $b_P \approx -3.1$ which are $O(1)$ quantities compared to $\sqrt{\gamma}$. Equations (A7)–(A9) then simplify as

$$\frac{dI_a}{ds} = (n_0 + \sqrt{2} b_L^2 n_c) I_a, \quad (\text{A11})$$

$$\frac{dn_0}{ds} = A_0(1 + \beta_L) - 1 - \frac{1 + \beta_L}{2} I_a + O(\sqrt{\gamma}), \quad (\text{A12})$$

$$\frac{dn_c}{ds} = \sqrt{\gamma} \left[-\frac{A b_P}{2 b_L} - \frac{1}{1 + \beta_L} \frac{1}{4} I_a - n_c \left(1 + \frac{1 + \beta_L}{2} I_a \right) \right] + O(\sqrt{\gamma}). \quad (\text{A13})$$

Equation (A13) implies that n_c is a constant in first approximation. On the other hand, Eqs. (A11) and (A12) form a conservative system of equations that admits a one-parameter family of periodic solutions. This can be demonstrated in the phase plane by determining a first integral from the equation dn_0/dI_a which is separable. From now on, we denote by (I_a, n_0) , the P -periodic solution of Eqs. (A11) and (A12). In order to find how n_c slowly changes in time, we apply the method of multiple time scales and construct a solution that depends on both the relaxation oscillations time s and the slow time $\sigma = \sqrt{\gamma} s$. These two times are assumed independent which imply the chain rule

$$\frac{dn_c}{ds} = (n_c)_s + \sqrt{\gamma} (n_c)_\sigma, \quad (\text{A14})$$

as well as similar expressions for dI_a/ds and dn_0/ds . The subscripts s and σ mean partial derivatives. We only analyze Eq. (A13). Specifically, we seek a solution of Eq. (A13) of the form

$$n_c = n_{c0}(s, \sigma) + \sqrt{\gamma} n_{c1}(s, \sigma) + \dots \quad (\text{A15})$$

Substituting (A15) into Eq. (A13), we find that the two first problems are $(n_{c0})_s = 0$ and

$$(n_{c1})_s = - (n_{c0})_\sigma - \frac{A b_P}{2 b_L} - \frac{1}{1 + \beta_L} \frac{1}{4} I_{a0} - n_{c0} \left(1 + \frac{1 + \beta_L}{2} I_{a0} \right). \quad (\text{A16})$$

The equation for n_{c0} implies that $n_{c0} = n_{c0}(\sigma)$ is only a function of the slow time σ . Equation (A16) is an equation for n_{c1} that only appears on the left-hand side. The right-hand side is a P -periodic function of s because of I_{a0} is P periodic. In order to have a bounded solution for n_{c1} with respect to s , the average of the right-hand side needs to be zero. This condition leads to a differential equation for n_{c0} given by

$$\frac{dn_{c0}}{d\sigma} = -\frac{A b_P}{2 b_L} - \frac{1}{1 + \beta_L} \frac{1}{4} \langle I_{a0} \rangle - n_{c0} \left(1 + \frac{1 + \beta_L}{2} \langle I_{a0} \rangle \right), \quad (\text{A17})$$

where

$$\langle I_{a0} \rangle \equiv \frac{1}{P} \int_0^P I_a(s, \sigma) ds. \quad (\text{A18})$$

We next wish to evaluate $\langle I_{a0} \rangle$. To this end, we integrate Eq. (A12) for 0 to P and obtain

$$\left\langle \frac{dn_0}{ds} \right\rangle = A_0(1 + \beta_L) - 1 - \frac{1 + \beta_L}{2} \langle I_a \rangle, \quad (\text{A19})$$

where

$$\left\langle \frac{dn_0}{ds} \right\rangle \equiv \frac{1}{P} \int_0^P \frac{dn_0}{ds} ds = \frac{1}{P} \int_0^P dn_0 = 0, \quad (\text{A20})$$

because n_0 is P periodic.. Consequently, Eq. (A19) leads to the following expression of $\langle I_a \rangle$:

$$\langle I_a \rangle = \frac{2}{1 + \beta_L} [A_0(1 + \beta_L) - 1]. \quad (\text{A21})$$

Introducing (A21) into Eq. (A17), we obtain

$$\frac{dn_{c0}}{d\sigma} = -\frac{Ab_P}{2b_L} - \frac{1}{2(1 + \beta_L)^2} [A_0(1 + \beta_L) - 1] - n_{c0}A_0(1 + \beta_L). \quad (\text{A22})$$

In terms of the original variables and parameters, the equation that describes the slow evolution of N_c is given by

$$\frac{dN_c}{ds} = \sqrt{\gamma} \left(-\frac{A(\beta_P - 1)}{2} - \frac{1 - \beta_L}{2(1 + \beta_L)^2} [A_0(1 + \beta_L) - 1] - N_c A_0(1 + \beta_L) \right). \quad (\text{A23})$$

In summary, N_c has an exponential evolution according to Eq. (A23) while E_a and N_0 exhibit relaxation oscillations on the fast time scale s . This is in agreement with the simulation results presented in Sec. III C. How long is the silent phase during which I_b remains close to zero depends on the stability of $I_b=0$. We examine this question in the next section.

2. Stability of $I_b=0$

In order to determine when I_b will jump from zero, we need to integrate its equation. From Eq. (3) and using (A4)–(A6), this equation is given by

$$\frac{dI_b}{ds} = (n_0 - \sqrt{2}b_L^2 n_c) I_b. \quad (\text{A24})$$

Equation (A24) is separable and admits the solution

$$I_b = I_b(0) \exp \left[\int_0^s (n_0 - \sqrt{2}b_L^2 n_c) ds \right]. \quad (\text{A25})$$

Using Eq. (A11), We may determine the integral of n_0 as

$$\int_0^s n_0 ds = -\sqrt{2}b_L^2 \int_0^s n_c ds + \int_0^s \frac{d \ln(I_a)}{ds} ds. \quad (\text{A26})$$

We next recall that $n_c = n_{c0}(\sigma)$ in the first approximation, where $\sigma \equiv \sqrt{\gamma} s$. This implies that

$$\int_0^s n_0 ds = -\sqrt{\frac{2}{\gamma}} b_L^2 \int_0^\sigma n_{c0}(\sigma') d\sigma' + \ln \left(\frac{I_a(s)}{I_a(0)} \right). \quad (\text{A27})$$

The first term on the right-hand side of Eq. (A26) dominates as $\gamma \rightarrow 0$ which implies that (A25) reduces to

$$I_b = I_b(0) \exp \left(-2 \sqrt{\frac{2}{\gamma}} b_L^2 \int_0^\sigma n_{c0}(\sigma') d\sigma' \right). \quad (\text{A28})$$

We next rewrite the integral on the right-hand side of Eq. (A28) as

$$\int_0^\sigma n_{c0}(\sigma') d\sigma' = \int_0^{\sigma_0} n_{c0}(\sigma') d\sigma' + \int_{\sigma_0}^\sigma n_{c0}(\sigma') d\sigma', \quad (\text{A29})$$

where σ_0 corresponds to $n_{c0}(\sigma_0)=0$. The expression (A28) may then be rewritten as

$$I_b = I_b(0) \exp \left(-2 \sqrt{\frac{2}{\gamma}} b_L^2 [F(\sigma) - F(0)] \right). \quad (\text{A30})$$

where

$$F(\sigma) \equiv \int_{\sigma_0}^\sigma n_{c0}(\sigma') d\sigma'. \quad (\text{A31})$$

The critical time $\sigma = \sigma_c$ where I_b changes from an exponentially small [$\exp(-\gamma^{-1/2})$] to an exponentially large [$\exp(\gamma^{-1/2})$] quantity occurs when the growth rate changes sign. From (A30), we find that $\sigma = \sigma_c$ is the nonzero root of

$$F(\sigma) - F(0) = 0. \quad (\text{A32})$$

In summary, the change of stability does not occur at $\sigma = \sigma_0$ where N_c changes sign but is delayed to $\sigma = \sigma_c$. The latter satisfies the integral condition (A32) or equivalently

$$\int_{\sigma_0}^{\sigma_c} N_c(\sigma) d\sigma = \int_{\sigma_0}^{\sigma_0} N_c(\sigma) d\sigma. \quad (\text{A33})$$

The integral condition (A33) physically means that I_b is exponentially close to zero and needs the same amount of time to leave the unstable zero solution as it took to approach the stable zero solution. This condition defined the delay of the bifurcation transition located at $N_c=0$. If noise of amplitude δ is added to the equation for E_b , this delay is reduced but occurs only if $\delta \geq \exp(-1/\gamma)$.

- [1] D. Lenstra, *Phys. Rep.* **59**, 299 (1980).
- [2] J. C. Cotteverte, F. Bretenaker, A. Le Floch, and P. Glorieux, *Phys. Rev. A* **49**, 2868 (1994).
- [3] M. D. Matlin, R. S. Gioggia, N. B. Abraham, P. Glorieux, and T. Crawford, *Opt. Commun.* **120**, 204 (1995).
- [4] S. Bielawski, D. Derozier, and P. Glorieux, *Phys. Rev. A* **46**, 2811 (1992).
- [5] R. Dalgliesh, A. May, and G. Stephan, *IEEE J. Quantum Electron.* **34**, 1485 (1998).
- [6] M. Brunel, O. Emile, M. Alouini, A. Le Floch, and F. Bretenaker, *Phys. Rev. A* **59**, 831 (1999).
- [7] H. Zeghlache and A. Boulnois, *Phys. Rev. A* **52**, 4229 (1995).
- [8] R. Leners and G. Stephan, *Quantum Semiclass. Opt.* **7**, 757 (1995).
- [9] G. Giacomelli, F. Marin, and I. Rabbiosi, *Phys. Rev. Lett.* **82**, 675 (1999).
- [10] M. B. Willemsen, M. P. van Exter, and J. P. Woerdman, *Phys. Rev. Lett.* **84**, 4337 (2000).
- [11] G. Verschaffelt, J. Albert, I. Veretennicoff, J. Danckaert, S. Barbay, G. Giacomelli, and F. Marin, *Appl. Phys. Lett.* **80**, 2248 (2002).
- [12] B. Nagler *et al.*, *Phys. Rev. A* **68**, 013813 (2003).
- [13] D. M. Grasso and K. Choquette, *IEEE J. Quantum Electron.* **41**, 127 (2005).
- [14] G. Verschaffelt, K. Panajotov, J. Albert, B. Nagler, M. Peeters, J. Danckaert, I. Veretennicoff, and H. Thienpont, *Opto-Electron. Rev.* **9**, 257 (2001).
- [15] M. San Miguel, Q. Feng, and J. V. Moloney, *Phys. Rev. A* **52**, 1728 (1995).
- [16] G. Van der Sande, M. Peeters, I. Veretennicoff, J. Danckaert, G. Verschaffelt, and S. Balle, *IEEE J. Quantum Electron.* **42**, 896 (2006).
- [17] R. Goidin, V. Kichuk, N. Kravtsov, G. Laptev, E. Lariontsev, and V. Firsov, *Quantum Electron.* **28**, 347 (1998).
- [18] P. Dekker and J. M. Dawes, *J. Opt. Soc. Am. B* **15**, 247 (1998).
- [19] M. Alouini, F. Bretenaker, M. Brunel, A. Le Floch, M. Vallet, and P. Thony, *Opt. Lett.* **25**, 896 (2000).
- [20] G. Bouwmans, Ph.D. thesis, 2001, <http://tel.ccsd.cnrs.fr/tel-00083926>
- [21] M. Brunel, A. Amon, and M. Vallet, *Opt. Lett.* **30**, 2418 (2005).
- [22] E. Lariontsev and I. Zolotoverh, *Opt. Commun.* **249**, 523 (2005).
- [23] G. Bouwmans, B. Ségard, P. Glorieux, P. A. Khandokhin, N. D. Milovsky, and E. Y. Shirokov, *Radiophys. Quantum Electron.* **47**, 729 (2004).
- [24] G. Bouwmans, B. Ségard, and P. Glorieux, *Opt. Commun.* **196**, 257 (2001).
- [25] S. Singh, R. Smith, and L. Van Uitert, *Phys. Rev. B* **10**, 2566 (1974).
- [26] G. Spuhler, R. Paschotta, R. Fluck, B. Braun, M. Moser, G. Zhang, E. Gini, and U. Keller, *J. Opt. Soc. Am. B* **16**, 376 (1999).
- [27] P. Mandel and T. Erneux, *Phys. Rev. Lett.* **53**, 1818 (1984).